

Assessing volumetric change distributions and scaling relations of retrogressive thaw slumps across the Arctic

Philipp Bernhard¹, Simon Zwieback², Nora Bergner¹, and Irena Hajsek^{1,3}

¹Institute of Environmental Engineering, ETH Zurich, 8093 Zurich, Switzerland ETH Zürich

²Geophysical Institute, University of Alaska Fairbanks, Fairbanks, AK 99775 USA

³Microwaves and Radar Institute, German Aerospace Center (DLR) e.V., 82234 Wessling, Germany

Correspondence: Philipp Bernhard (bernhard@ifu.baug.ethz.ch)

Abstract. Arctic ice-rich permafrost is becoming increasingly vulnerable to terrain altering thermokarst, and among the most rapid and dramatic of these changes are retrogressive thaw slumps (RTS). They initiate when ice-rich soils are exposed and thaw, leading to the formation of a steep headwall which retreats during the summer months. The impacts and the distribution and scaling laws governing RTS changes within and between regions are unknown. Using TanDEM-X-derived digital elevation models, we estimated RTS volume and area changes over a 5-year period and use probability density functions to describe their distributions. We contrasted 10 regions study sites (Eurasia: 5, North America: 5), with a total size of 220 000 km³, ~~and over that time~~. Over the 5-year time-period all 1853 RTSs combined mobilized a total volume of $17 \cdot 10^6 \text{ m}^3 \text{ yr}^{-1}$ ~~m³ yr⁻¹~~ corresponding to a volumetric change density of $77 \text{ m}^3 \text{ yr}^{-1} \text{ km}^{-2}$ ~~m³ yr⁻¹ km⁻²~~. Our remote sensing data revealed inter-regional differences in mobilized volumes, scaling laws and terrain controls. The distributions of RTS area and volumetric change rates followed an inverse gamma function with a distinct peak and an exponential decrease for the largest RTSs. We found that the distributions in the high Arctic were shifted towards larger values. The area-to-volume scaling could be well described by a power law with an exponent of 1.15 across all regions study sites, however the individual regions sites had scaling exponents ranging from 1.05 to 1.37, indicating that regional characteristics need to be taken into account when estimating RTS volumetric changes from area changes. ~~The distributions of RTS area and volumetric change rates followed an inverse gamma function with a distinct peak and an exponential decrease for the largest RTSs~~. We found that the distributions in the high Arctic were shifted towards larger values. Among the terrain controls on RTS distributions that we examined, slope, adjacency to waterbodies and aspect, the latter showed the greatest, but regionally variable association with thaw slump occurrence. Accounting for the observed regional differences in volumetric change distributions, scaling relations and terrain controls may enhance the modelling and monitoring of Arctic carbon, nutrient and sediment cycles.

20 1 Introduction

About 15 % of the landmass in the northern Hemisphere is underlain by permafrost (Obu, 2021). With climate warming these permafrost regions become increasingly vulnerable to ~~rapid thaw~~(Grosse et al., 2011; Schuur et al., 2015). ~~Rapid permafrost degradation has~~ thaw. This thaw manifest itself first in a slow but gradual deepening of the seasonally thawed active layer (press disturbances) and secondly in a more rapid and local way by the development of thermokarst features (pules disturbances) (Grosse et al., 2011; Schuur et al., 2015). Both forms of permafrost degradation have major impacts by changing ecosystem and hydrological equilibria. ~~Furthermore, it can and~~ impact the Earth system on a global scale by reinforcing climate change with the additional mobilization of organic carbon that was previously stored in the frozen soil. One important ~~land surface characteristic arising from rapid thaw~~ thermokarst feature arising from pulse disturbances are retrogressive thaw slumps (RTS). These ~~slumps~~ RTSs initiate by the exposure of ice-rich soils with a subsequent thaw and the formation of a steep headwall (Burn and Lewkowicz, 1990; Kokelj et al., 2009). During the summer, the ice in the headwall melts which leads to a continuous retreat. This process can mobilizes vast quantities of sediments on ~~a short time scale~~ time scales of years. In the context of recent climate warming an increase in the number and sizes of RTSs in permafrost regions has been found (Lantz and Kokelj, 2008; Lantuit and Pollard, 2008; Gooseff et al., 2009; Kokelj et al., 2009; Lewkowicz and Way, 2019). However, the inter-regional differences in the rates of thaw slumping in terms of their magnitude, distribution and controls remain poorly constrained and so are the implications for carbon and nutrient cycles.

For the investigation of landslides in temperate climate zones, frequency distributions and scaling laws of various form have been used to quantify hazards and ecosystem impacts as well as to improve the process understanding of landslide activity (Tebbens, 2020). The variability and similarities of these laws in terms of landslides properties and area characteristics have played an important role. The soil properties (ice-content) as well as timescales (single event vs. polycyclic multi-year retreat) are different for RTSs than other landslides, but nevertheless the methods used as well as the universality of landslides characteristics could provide valuable insights into RTS drivers and controls. Furthermore, due to the strong spatial variability of soil-carbon densities as well as RTS activity past model estimates of the impacts of RTSs on the carbon cycle have large uncertainties (Turetsky et al., 2020). Currently there is only one study quantifying the area frequency distributions of RTSs, were orthophotos for a study site on Svalbard was used to measure the area disturbed by RTSs (Nicu et al., 2021). Quantifying the RTS frequency distributions and scaling laws as well as their variability across regions have the potential to greatly improve future carbon release rates.

Two of the most common methods to describe landslides are the frequency distribution as well as the area-to-volume scaling. For the frequency distribution the area (or volume) change of the erosion site showing elevation loss is used. In this distribution typically two parts can be distinguished, an exponential decay part describing larger landslides and a deviation from this power-law for smaller events with a distinct peak, indicating the most common landslides in the region. The exponential decay part is well explained by models that merge closely proximal landslides. The attribution of the deviation from the power law is more controversial and is either attributed to an under-sampling of small events or to real physical processes (Tanyaş et al., 2018). The second scaling law, namely the area-to-volume scaling, is based on an observational relation between land-

slide area and volumetric change. Many studies of landslides inventories that include different sizes, slope failure mechanisms and locations show that area-to-volume scaling follows a power law relation $V \propto A^\gamma$ with γ ranging from 1 to 1.5. (Larsen et al., 2010). In a pure mathematical sense, a γ of 1.5 corresponds to a situation where objects scale in an invariant way, meaning that if the height dimension is increased by a certain amount, the horizontal (area) dimension is increased by the same. Consequently a scaling coefficient smaller than 1.5 corresponds to a situation where an increase in area leads to a smaller but proportional increase in height (Klar et al., 2011). The ability to estimate the volumetric change from area measurements can especially be useful for estimating the amount of mobilized material if only area measurement are available. Additionally, differences in γ between regions may suggest different physical drivers of RTS development.

To quantify these relations for RTSSs, remote sensing techniques are the most feasible due to the remote landscape and the severe climate conditions. Digital elevation models (DEMs) that cover the pan-Arctic permafrost terrain with a high enough resolution to study RTSSs only became available in the last few years. One of these high resolution DEMs is based on single-pass InSAR observations taken by the TanDEM-X satellites. TanDEM-X is a high-resolution single-pass interferometry satellite mission that was launched by the German Aerospace Center (DLR) with the purpose of generating a high resolution global DEM (Krieger et al., 2007). The satellite pair started observations in 2010 and have observed the global land mass two to three times, now. The expected spatial resolution of about 10 to 12 m and vertical height resolutions of the order of about 2 to 3 m is smaller than typical RTS change rates and can thus provide accurate estimates of the thaw slump topography as well as related controls on RTS processes like aspect, slope, and location (Bernhard et al., 2020).

In this study we use DEMs generated from TanDEM-X observations to derive the volume and area change rates of RTSSs of several Arctic regions. Additionally we derive several terrain controls namely the aspect, slope, and location. This work focuses on answering the following questions:

1. Does the area and volume change probability density function of RTSSs follow the typical landslide distribution and to what extent does the function vary across regions/sites?
2. What are the area-to-volume scaling law coefficients for the study regions/sites and are they different?
3. Do the terrain controls vary between regions/sites, and if so is the variation related to thaw slumps/RTS size?

The large number of thaw slumps/RTSSs in our sample and the diverse nature of our study regions/sites allow for a robust statistical inference in answering these questions. The results should provide valuable insights concerning susceptibility modelling and will further improve our understanding of the process that govern RTS initiation and growth as well as their future impact on ecological and hydrological systems.

2 Study Regions/Sites

We chose 10 different study sites located in permafrost regions across the Arctic (Figure 1). The selection was first based on regions/sites where previous studies have shown RTS activity: the Peel Plateau and Richardson Mountains ("Peel"), Banks Island ("Banks"), the western Mackenzie River Delta uplands and Tuktoyaktuk Coastlands ("Tuktoyaktuk") and Ellesmere

Island ("Ellesmere") that are all located in northern Canada, the Noatak Basin ("Noatak") in Alaska, and the Yamal and Gydan Peninsula in Siberia (Lacelle et al., 2010; Balsler et al., 2014; Segal et al., 2016; Nitze et al., 2017; Jones et al., 2019; Nesterova et al., 2019). Additionally, we chose three study regions-sites in Siberia that exhibit RTS activity but are not well studied, namely on the Taymyr Peninsula ("Taymyr 1 and 2") and on the Chukotka Peninsula ("Chukotka").

- 90 The study regions-sites are located in the Arctic tundra and the boreal-tundra transition regions within the continuous permafrost zone (Brown et al., 2002). They show differences in environmental properties including permafrost type, topography, lake-abundance, and vegetation type. ~~Due to the large extent of some areas we selected only parts as our study region~~ Within these extensive regions we selected representative locations for our study sites. The exact outline of the study regions-sites were based on the Sentinel-2 tiling to facilitate the data processing steps.
- 95 The amount of ground ice on a pan-arctic scale has not been well characterized, but estimations on coarse scale report ground ice contents of >10% for all study regions-sites (Brown et al., 2002). On large scales, high ground ice content is associated with the climatic history (e.g. syngenetic ice-wedges) and the associated extent of past glacial ice (e.g. buried glacial ice). On small scales ground ice content ~~varies strongly can vary~~ due to for example ~~topography or~~ soil type (Lacelle et al., 2004). ~~The study regions-~~
- 100 The study sites on Peel, Banks, Ellesmere, Noatak and Chukotka show strong variation in topography with elevation changes of several hundred meters inside the study regions-sites. The remaining regions-sites show only small variation in elevation (<100m). Another difference between the study regions-sites is in the amount of lakes present. The study region-site with the most abundance of lakes are in Tuktoyaktuk and Taymyr 2. Only small amounts of lakes are found on Ellesmere and in Noatak (Table 1).

Table 1. Overview of study sites with size, lake area percentage, elevation range, and number of processed TanDEM-X observations.

<u>Study Regions-sites</u>	Size [10^3km^2]	lake area <u>Lake area [%]</u>	Elevation [m]	TanDEM-X obs. [N]
Peel	19.3	4.3 %	100 - 1500	307
Banks	6.6	6.3 %	0 - 400	62
Tuktoyaktuk	7.7	14.7 %	< 100	87
Ellesmere	9.5	2.2 %	0 - 650	164
Noatak	16.3	1.5 %	400 - 1400	134
Yamal	24.8	6.0 %	< 100	143
Gydan	14.6	8.9 %	< 100	87
Taymyr 1	23.6	4.1 %	< 100	128
Taymyr 2	11.0	11.1 %	< 100	124
Chukotka	87.9	1.4 %	0 - 1100	262

~~Overview of study regions with size, lake area percentage, elevation range and number of processed TanDEM-X observations. The lake area percentage was calculated using the generated waterbody mask. Open waterbodies were not included in the calculation. Note: The lake area percentage was calculated using the generated waterbody mask. Open waterbodies were not included in the calculation.~~



Figure 1. Overview of the study regionssites. The study regions-sites are distributed around the Arctic with four study regions-sites in northern Canada, one located in Alaska and five in Siberia. The purple area shows the zone of continuous permafrost region-(Brown et al., 2002).

3.1 Data and Processing

For the DEM generation we used TanDEM-X observations acquired between 2010 and 2017. To ensure adequate vertical accuracies, we only used acquisitions with a height of ambiguity smaller than 80 m (Martone et al., 2012). The radar incidence angles range from 36° to 44° . For an accurate orthorectification we used the TanDEM-X 12m DEM as reference and iteratively ~~update~~ updated the look-up table based on the measured deviation (Leinss and Bernhard, 2021). We only studied winter acquisitions. ~~Due to, because outside the winter months thawed vegetation, wet snow and standing water induce sizeable errors (Bernhard et al., 2020), whereas in winter we expect~~ the low average monthly temperature ~~we can expect to produce~~ a dry snow-pack and radar waves can propagate through to the ground without being strongly affected (Millan et al., 2015; Leinss and Bernhard, 2021). ~~Outside the winter months thawed vegetation, wet snow and standing water induce sizeable errors (Bernhard et al., 2020).~~ For the DEM generation we followed a standard approach (Fritz et al., 2011). The resulting DEMs have a planimetric resolution of about 10 ~~to 12~~ -12m-m and vertical accuracies of about 2m in areas with high coherences. The interferometric processing was done using the *Gamma Remote Sensing* software (Werner et al., 2000). More processing details including tilt-removal and correction of misalignments, specifically for DEMs generated from ~~InSAR~~ interferometric SAR observations in permafrost regions can be found in Bernhard et al. (2020).

3.2 RTS detection and manual mapping of affected areas

DEM's corresponding to the same winter were averaged and mosaicked. We then used an automated detection algorithm to identify significant elevation changes in the DEM difference images from DEMs that were obtained more than 3 years apart (Bernhard et al., 2020). For each detection several processing steps were carried out. First the topography and environment were assessed using a TanDEM-X DEM and Sentinel-2 multispectral images taken in summer (snow-free). For all study ~~regions~~ sites at least one Sentinel-2 image during the years 2016 to 2019 was available. The criteria for classifying a detection as an active RTS were the exposure of bare soils, a retreat over time, a location related to a potential sediment removal mechanism, and the presence of a headwall (Lantuit and Pollard, 2008; Nitze et al., 2018; Lewkowicz and Way, 2019). In uncertain cases additional time-series of Planet Rapid-Eye optical data was used to classify the detections (Planet-Team, 2018).

The ~~lower limit for a RTSs to be detectable~~ error sources and uncertainties that govern the lower RTS detection limit in terms of headwall height and retreat ~~is very hard to quantify~~ rate are manifold and difficult to quantify. This is mainly due to the ~~limited~~ small amount of available high resolution, three dimensional RTS inventories. ~~Here also the timescales (Swanson and Nolan, 2018; Van der~~ , were also time-scales on which the RTSs are monitored plays an important role. ~~The 90th percentile in terms of elevation changes of the~~ To get an estimate on the lower limit of RTS induced elevation changes to be detectable we can analyse the smallest detected RTSs in our sample. The 10 smallest detected RTSs ~~is~~ have elevation changes in the range of ~~1.6m-1.6~~ to 1.9m and can be seen as an approximation for the smallest RTS headwall heights that are detectable, which are on the same order then the general TanDEM-X DEM accuracies. Similarly, the smallest total area changes of detected RTSs are on the order of ~~500m²-500~~ to 1000m². ~~If,~~ corresponding to about 10 to 12 pixels. Consequently, if the size of the erosion features

approaches the pixel resolution also the accuracy of the estimated volume loss increases. ~~Here InSAR-related processes play the biggest role like~~ Additionally, processes related to the observation properties and interferometric processing further complicate the error estimations. For example the about 40 degree right looking viewing geometry ~~in an ascending orbit and inaccuracies in the estimated coherence~~ leads to different pixels resolution depending on aspect and slope of the observed area. These error sources and increased uncertainties especially for small RTSs, both in terms of spatial and vertical changes, should be considered in the interpretation and future use of the dataset.

After the classification step we generated polygons for each detected RTS outlining the area with significant elevation change. Examples of the generated polygons are shown in the Supplement (Figures ~~S1-S4~~). ~~An automated method using a fixed threshold on the elevation change gave unreliable results. Thus the S1 to S4~~. The polygons outlining the area of elevation change were drawn by a trained student and the first author. ~~Additionally, the location of the RTSs, as our use of an automated method that implemented a fixed threshold on the elevation change gave unreliable results. The RTS polygons were attributed in terms of location as either "shoreline" (located close to a waterbody) or "hillslope" (located at trenches or riverbeds) was noted.~~

3.3 RTS attributes

For all calculations we used the ~~area outlined by the polygon indicating the areas showing an polygon, which indicate an area of elevation change and thus a net volume loss. It is to~~ We note that this area can also ~~be include~~ a zone of deposition, especially for small and low-relief RTSs or if the time between observations increases. ~~Areas~~ We could not accurately detect areas such as the debris tongues or zones of alluvial deposits ~~can not be accurately detected by the DEM difference data and and they~~ are not included. We computed the volumetric and area change as well as the slope and aspect. ~~In some cases observations during several~~ For parts of the study sites observations during winters in 2010/11, 2011/12 and/or 2012/13 were available. To simplify the analysis we normalized the properties to changes per year and took the average if several DEM difference pairs were available. It is important to note that unlike most landslides, RTSs are multi-year features with a strong variability in the erosional intensity as well as a potential change of their morphology over time. In the interpretation of the results and specifically the comparison to landslide studies, the use of the integrated change over several years needs to be considered. We computed the aspect and slope by using the pre-disturbed elevation model and applied gaussian smoothing with a standard deviation corresponding to 100 m to reduce the influence of random errors (Kang-tsung and Bor-wen, 1991). For the aspect distribution we additionally computed the aspect distribution weighted by volume.

To quantify the volumetric change rate density (volumetric change rate per unit area) we first use a simple approach by dividing the summed total of all RTS volumetric changes per year by the study ~~region site~~ size. This has a drawback because RTSs often occur heterogeneously and the result strongly depends on the exact outline of the study ~~region sites~~ (Ramage et al., 2017). For example, in the Peel study ~~region site~~ only the east facing part of the mountain range experiences RTS development, but our study ~~region site~~ also includes the western part of the range where nearly no RTS activity was detected. To account for this problem we follow a similar approach than proposed in Kokelj et al. (2017) and divide our study ~~region site~~ into tiles of sizes ~~10 km x 10 km~~ 10 km by 10 km and counted the number of empty grid cells and computed a more representative RTS density

using only the cells showing RTS activity. It is to note that to interpret the computed density values the number of empty as well as the number of non-empty grid cells in relation to the total size of the study region-site should be considered.

To quantify the amount of lakes in each study region-site we used the waterbody mask generated from Sentinel-2 data and computed the area that is covered by the mask (McFeeters, 1996; Kaplan and Avdan, 2017). For this computation, we excluded open sea areas.

We investigated the dependency of RTS growth on different terrain controls by computing the aspect, slope ~~and the location in terms of lakeshore- and hillslope-RTSs, and location (lakeshore or hillslope)~~. For the aspect we identified the most dominant orientation by summing the number of RTSs as well as the volumetric ~~and~~ area change rates in 8 aspect bins (N, NE, E, SE, S, SW, W, NW) and used these bins to compute the strength and orientation of the primary direction.

3.4 Change Rate Distributions

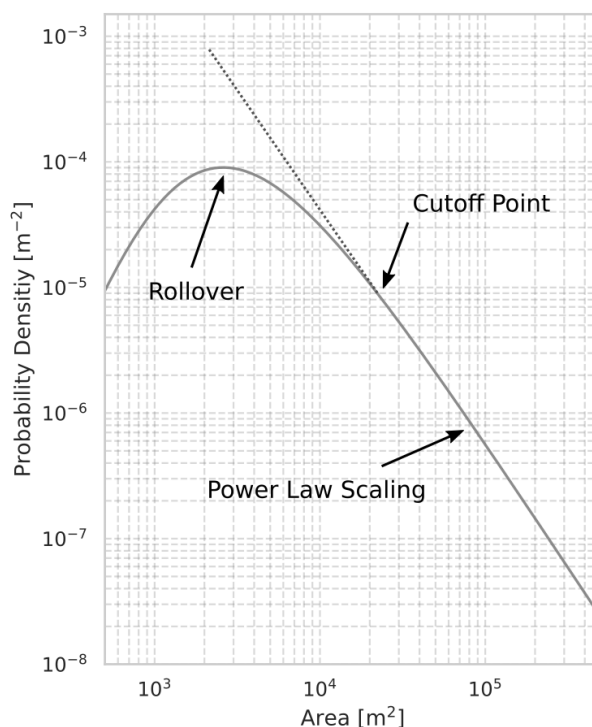


Figure 2. Schematic representation of RTS area probability density function. Two parts can be distinguished: An exponential decay part above the cutoff value and a deviation from the power-law scaling below the cutoff point.

The probability density function (PDF) of the area affected by elevation loss per year corresponding to an RTS inventory can be defined as

$$p(A_{RTS}) = \frac{1}{N_{RTS}} \frac{\delta N_{RTS}}{\delta A_{RTS}} \quad (1)$$

185 where A_{RTS} is the area change affected by elevation loss of a RTS per year, N_{RTS} the total number of RTS in the inventory, δN_{RTS} the number of RTS with affected areas between A_{RTS} and $A_{RTS} + \delta A_{RTS}$ and δA_{RTS} is the bin width. Equivalently the probability density function $p(V_{RTS})$ for the volumetric change per year can be defined.

All RTSs in the study show changes per year in the range of 10^2 to 10^6 m^2 yr^{-1} for the area and 10^2 to 10^6 m^3 yr^{-1} for the volume ~~and we thus we~~, and we used 30 bins sampled in log-space to cover these ranges.

190 When analysing a landslides PDF three quantities can be used to describe the distribution: the rollover- and cutoff-points for small events and the coefficient of the power law scaling β for large events. The rollover point is defined as the peak in the PDF and corresponds to the most common occurrence in the distribution. For large RTSs the PDF can be described as a power law function. The point at which the distribution starts to follow a power law is defined as the cutoff point (Figure 2).

To determine how well the data points are described by this model and to estimate the rollover point we fitted a three parameter
195 Inverse Gamma Function to the RTS probability density function (Malamud et al., 2004). To estimate the error of the fit we used the bootstrap method drawing 1000 random samples with replacement from all data points, and computed the R^2 value as well as the rollover point for each iteration (Ohtani, 2000).

For the computation of the cutoff value and the exponential scaling exponent we used the method proposed in of Clauset et al. (2009) which is commonly used in landslide frequency-area analyses (Bennett et al., 2012; Parker et al., 2015; Tanyaş
200 et al., 2018). The approach is based on sampling all possible cutoff values and estimating ~~corresponding the the corresponding~~ exponential scaling coefficients β using a maximum-likelihood fitting method. The obtained fitting values are then tested based on a Kolmogorov-Smirnov statistic and the values that follows best a true power law distribution are used as the final cutoff and β value. To quantify the uncertainty we again used a bootstrap algorithm.

3.5 Area-Volume scaling

205 One important quantity in comparing landslides of various sizes is ~~to relate the area to the volume change~~ the change relation between area and volume. The simplest conversion ~~assuming assumes that~~ an anisotropic scaling ~~with a scaling exponent γ~~ to relate ~~exponent α , which relates~~ the area and volume ~~$V \approx A^\gamma$ by: $V \approx A^\alpha$~~ . Since both variables (area and volume) are affected by measurement errors we used an orthogonal distance regression model to fit a straight line (Boggs and Rogers, 1990; Markovsky and Van Huffel, 2007). To quantify the goodness of the fit we calculated the RMSE, R^2 and p-value (in
210 log-space).

4 Results

We investigated 10 different study ~~regions-sites~~ and measured the area and volumetric change rates of 1854 RTSs over a ~~4–5~~ 4 to 5 year time-frame. Due to the low density of RTSs in Yamal and Gydan and the two study ~~regions-sites~~ in Taymyr we combined these to one study ~~region-site~~ (in the following "Yamal/Gydan" and "Taymyr") according to their geographical and geophysical proximity.

The number of RTSs per study ~~region-site~~ and the obtained volumetric change rates in terms of the total volume, ~~the density and the density, and~~ changes per RTS are shown in Table 2. We found the largest RTSs in terms of average volumetric change rates per RTS ~~on-at~~ Ellesmere, Peel, and Banks with yearly average change rates of $13\,200\text{ m}^3\text{ yr}^{-1}$, $12\,200\text{ m}^3\text{ yr}^{-1}$, and $10\,700\text{ m}^3\text{ yr}^{-1}$. The other areas show much smaller yearly average volumetric change rates in the the range of $2\,400\text{ m}^3\text{ yr}^{-1}$ (Tuktoyaktuk) to $3\,600\text{ m}^3\text{ yr}^{-1}$ (Taymyr). ~~RTSs-on~~ Compared to the other study sites, RTSs at Ellesmere, Peel, and Banks also show higher volumetric change both in terms of overall change per study ~~region-site~~ size (density) as well as per individual RTS. Furthermore, these three ~~regions-sites~~ also contain the largest overall size RTSs of the investigated study ~~regions-sites~~ (Figure 3).

In the following paragraphs we will present (1) a characterisation of the area and volumetric changes rates with special emphasis on the probability density functions with the estimation of the rollover, cutoff and exponential decay components; (2) the estimated area-to-volume scaling laws; and (3) several terrain controls that could potentially be related to RTS size and frequency. To compare the ~~estimated quantities in each section~~ quantities estimated in these three sections we computed the correlation coefficients between them.

Table 2. Number of RTSs in each study site with the total number of RTS and the volumetric change rates in terms of total change, density and average rates per RTS.

Area	N_{RTS} [N]	$V_{\text{change}}^{\text{total}}$ [$10^6\text{ m}^3\text{ yr}^{-1}$]	$V_{\text{change}}^{\text{mean}}$ (density) [$\text{m}^3\text{ yr}^{-1}\text{ km}^{-2}$]	$V_{\text{change}}^{\text{mean}}$ (RTS) [$10^3\text{ m}^3\text{ yr}^{-1}\text{ RTS}^{-1}$]
Peel Plateau-	438	5.27	342.8	12.2
Banks Island-	679	7.16	883.8	10.7
Ellesmere Island-	223	2.95	546.7	13.2
Tuktoyaktuk	212	0.5	43.3	2.4
Noatak	26	0.09	14.9	3.4
Yamal/Gydan	128	0.37	12.4	2.9
Taymyr	97	0.35	11.3	3.7
Chukotka peninsula	51	0.17	3.8	3.5

Number of RTSs in each study region

with the total number of RTS and the volumetric change rates in terms of total change, density and average rates per RTS.

4.1 RTS volume and area distributions

230 The estimated PDFs are shown in Figure 4a and 4b. For most areas the quality of fit of the inverse gamma function was good, as indicated by R^2 values > 0.80 . Exceptions were the Noatak and Chukotka study regions-sites with R^2 values between 0.6 and 0.7. These two regions-have-also-sites-also-have the lowest number of RTSs in the sample with only 26 (Noatak) and 51 (Chukotka) RTSs (Figure 4c and 4d).

The modes of the volume change distributions (rollover points) differ between regions-sites. The two study regions-sites located in the high Arctic (Ellesmere and BanksIsland) show an order of magnitude higher rollover values. The range of measured volumetric and area change rates show large variations for the Tuktoyaktuk and Peel study regions-sites, whereas the other study regions-show-only-small-variation-sites-show-smaller-variations.

The PDFs above the cutoff value, the relation between rollover and cutoff as well as the exponential decay values differ between regions-sites (Figure 5). For the PDF based on the volumetric change, a high rollover value is moderately associated with high cutoff values indicated by a correlation coefficient of 0.59 . By contrast, the PDF based on the area change rate shows a much stronger separation between the high Arctic regions-sites and the other study regions-sites and consequently also shows a high correlation factor of 0.98 . For the power law exponent for RTSs above the cutoff values no large difference between the areas is visible ($\beta \approx 2$ to 3 and correlation coefficients < 0.64). All correlation coefficients are shown in the Supplement (Figure S5). It is to note that for the yearly area and volumetric change rates the cutoff value for the Peel study region-site is relatively small but the distribution continues to high values with yearly area change rates of up to $26 \cdot 10^5 \text{m}^2 \text{yr}^{-1}$ and $10^4 \text{m}^2 \text{yr}^{-1}$ and $3 \cdot 10^6 \text{m}^3 \text{yr}^{-1}$ and $10^5 \text{m}^3 \text{yr}^{-1}$ (Mega-Slumps). The computed values of the rollover, cutoff, and exponential decay coefficients as well as the fit parameters for the inverse gamma function are reported in the Supplement Table-Tables S1 and S2.

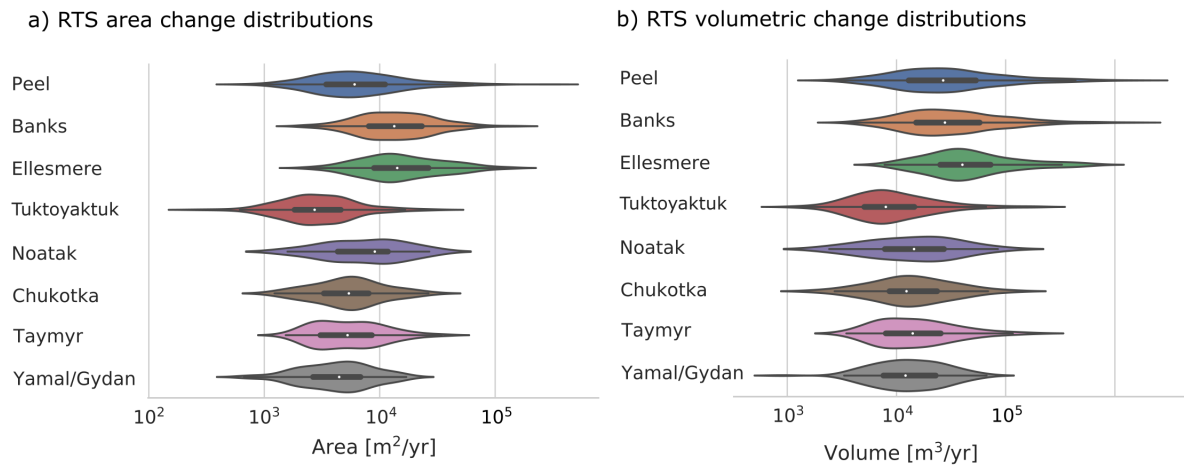
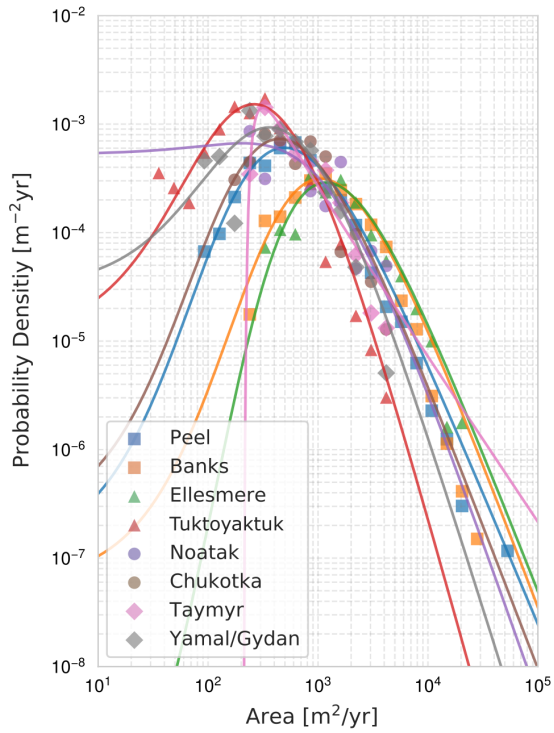
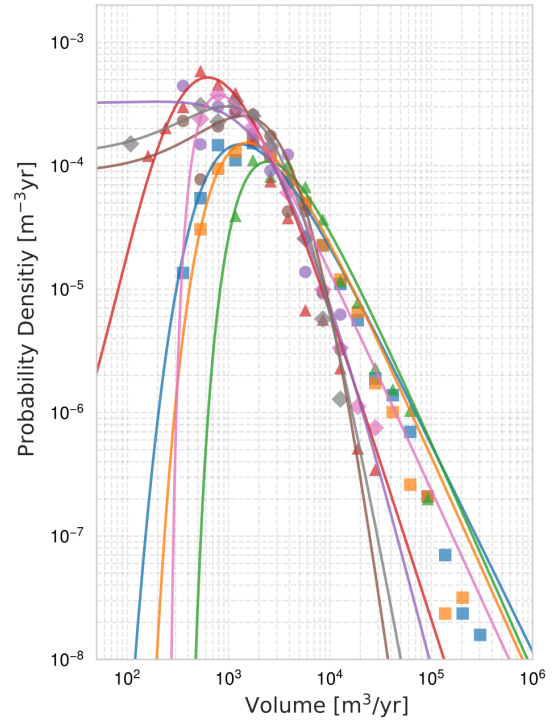


Figure 3. Area [a\)](#) and volumetric [b\)](#) change rate distributions of mapped RTSs. ~~a) and b) show the distribution of area and volumetric change rates~~ in form of violin plots. The white dots on the center lines indicate mean values for the set of study sites. For each violin plot the white dot on the center line indicates the mean value, the thick center line shows the interquartile range, the thin center line shows the total range of data, and the colored area indicates the probability density of the data across the distribution of values smoothed by a kernel density estimator.

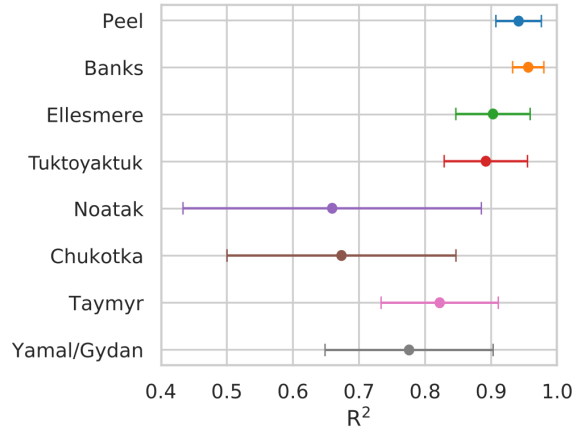
a) PDF of RTS area change



b) PDF of RTS volume change



c) Computed uncertainty (Area)



d) Computed uncertainty (Volume)

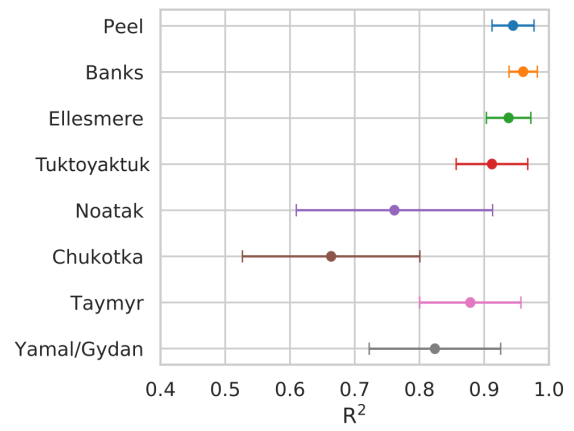


Figure 4. PDF of area and volumetric change rates of mapped RTSs [for the set of study sites](#). a) and b) ~~shows~~ ~~show~~ the ~~PDF~~ ~~PDFs~~ of area and volumetric change ~~rate~~ ~~rates~~ with fitted inverse gamma ~~function~~ ~~functions~~. c) and d) show the computed R^2 errors.

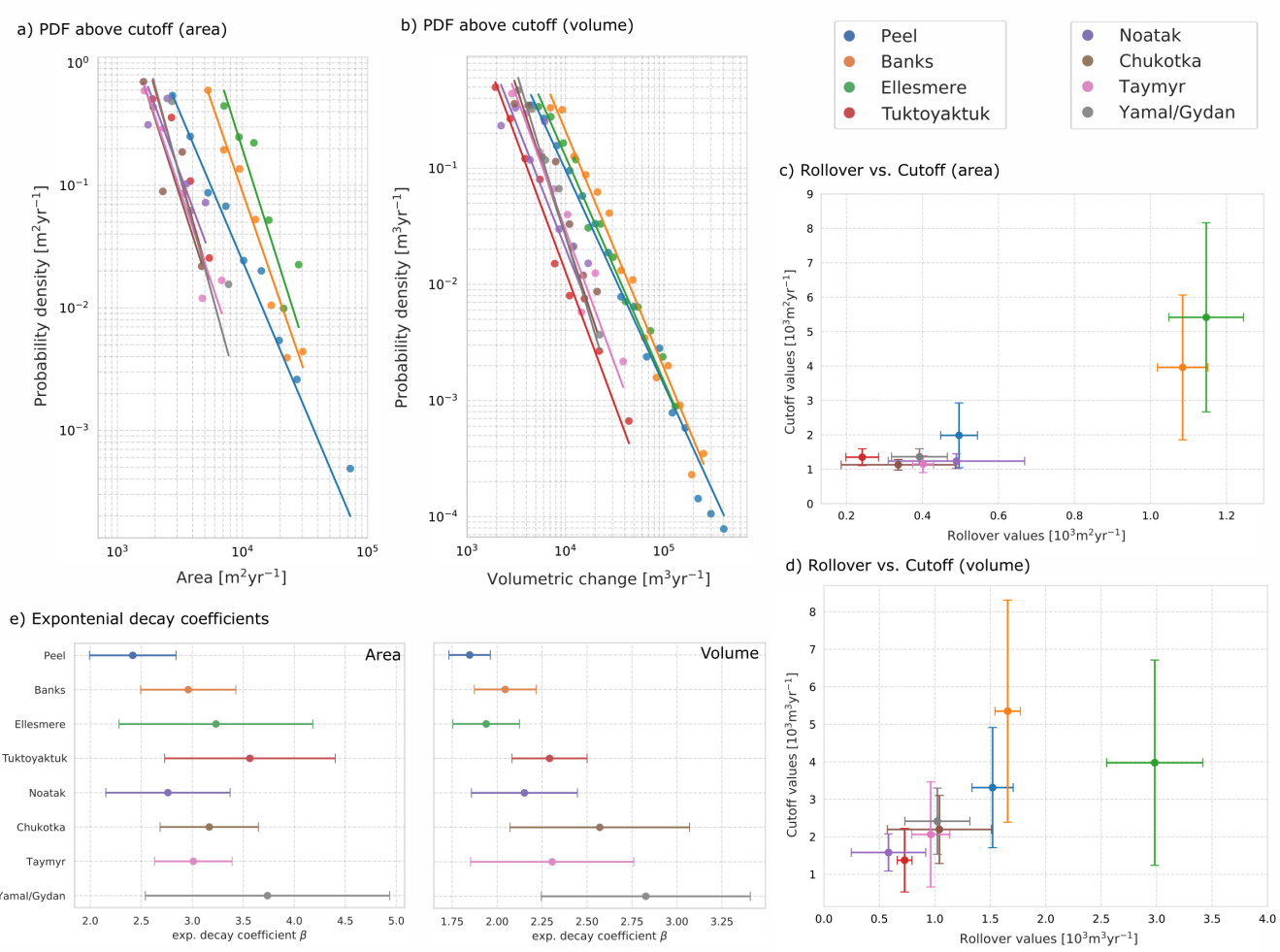


Figure 5. Cutoff, rollover, and exponential decay coefficients. a) and b) shows the PDFs for yearly area and volumetric change rates above the cut-off values. c) and d) shows the estimated rollover and cutoff values for yearly area and volumetric change rates. e) Exponential decay coefficients for fits above the cutoff.

4.2 Area-to-volume scaling

250 The estimated area-to-volume scaling law based on all data points in log-log space shows a clear relationship that spans over
four order of magnitudes orders of magnitude between the area and volumetric change rates (Figure 6a). The estimated scaling
exponent across all regions study sites was $\alpha = 1.15 \pm 0.01$. The quality of fit was decent, with a R^2 value of 0.81, RMSE of
0.21 m^3/yr m^3yr^{-1} and p-value smaller than 10^{-6} showing a strong dependency between RTS area and volumetric change
255 tings. Nevertheless we found a moderate inter-region variability in the scaling coefficient. The α coefficients for the individual
regions sites was in the range of 1.05 to 1.25 with the exception of RTSs in the Banks region site with a high coefficient of
1.37 (Figure 6b). The data points and fitted lines for each study region site individually can be seen in the Supplement Figure
S6. The strong association between area and volume scale change rates can facilitate the estimation of volume changes from
multispectral satellite images.

260

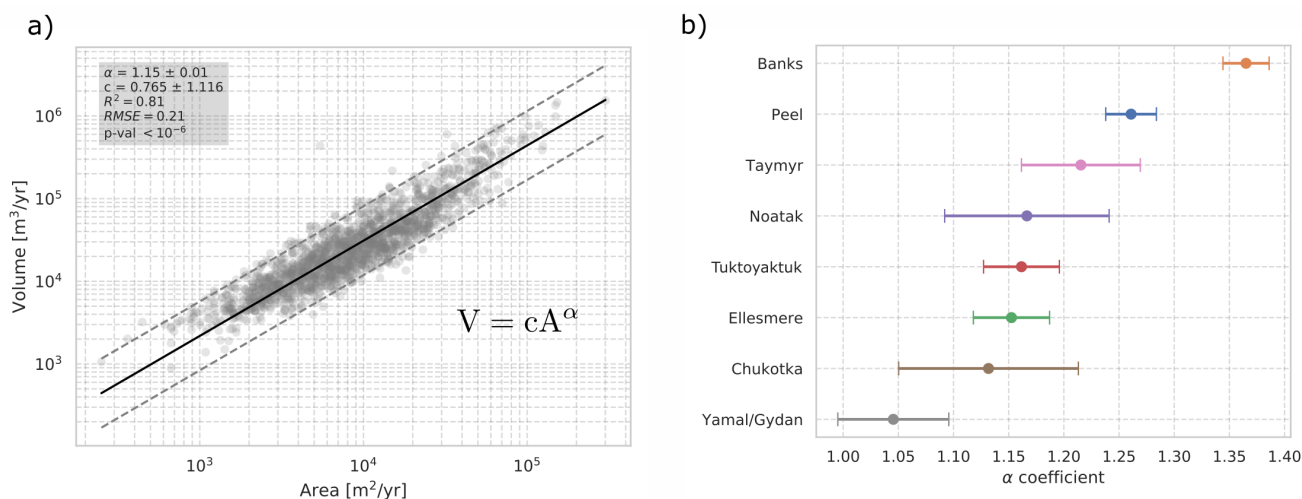


Figure 6. Area-to-volume scaling laws for RTS in the set of study sites. (a) shows the total dataset with all regions study sites combined. We found an exponential scaling exponent of $\alpha = 1.15 \pm 0.01$. (b) shows the computed values of the scaling exponent for each region site individually with the estimated standard deviation. A large variation between 1.05 and 1.37 is visible.

4.3 Terrain controls

Among the investigated terrain controls, aspect shows the greatest variability between ~~regions~~the study sites. RTSs located in Siberia as well as on Ellesmere tend to favour a South-West facing orientation (Figure 7a). The very small number of RTSs in the Noatak study ~~region~~site showed a preferred orientation towards the North-West and RTSs in Peel have a preferred orientation
265 towards the North-East. For Tuktoyaktuk and Banks no clear trend is visible. To consider the possibility of more than one preferred orientation we additionally looked at the initial aspect bin distribution (Supplement Figure S7). Here only the aspect distribution of RTSs in the Noatak valley shows two preferred orientation, but this could be related to the low number of RTSs in the study ~~regions~~site. Additionally to the number of RTSs in each aspect bin we weighted the aspect by the volumetric change rates. This does only slightly alter the preferred orientation and large RTSs do not occur at different aspects.

270 The slope of the pre-disturbed area shows some difference between the study ~~regions~~sites (Figure 7c). In general all RTSs evolve at slopes ranging from 2° ~~-3~~to 3° up to slopes of 20° . Interestingly, in the ~~region~~study site of the largest ~~slumps on Banks Island, RTSs~~RTSs on Banks, they tend to favour lower slopes with values below 12° .

We investigated the dependency of RTSs locations in terms of their occurrence. We distinguished two types of locations, either at a shore (including lake and coastal) or at hillslopes with no large waterbodies close by. Several ~~regions~~study sites have
275 mostly one type of RTS location. The RTSs in Ellesmere (99% hillslope), Peel (96% hillslope) and Noatak (88% hillslope) have mostly RTSs at hillslope locations. On the contrary, RTSs in the Tuktoyaktuk ~~region~~site are nearly all located at lakeshores (99%). All other ~~regions~~study sites have a mixture of hillslope and shoreline RTS locations: Banks (66% hillslope), Chukotka (52% hillslope), Taymyr (27% hillslope) and Yamal/Gydan (26% hillslope). In the ~~regions~~study sites with both types of RTS locations no significant difference between the distributions is visible (Figure 7c). Furthermore, we did not find a significant
280 correlation between RTS size and the percentage of hillslope or shoreline RTS locations (Supplement Figure S5).

To estimate the volumetric change rate density of RTSs within the RTS-affected regions of each study ~~region~~site we gridded them into tiles of size 10 km ~~×~~by 10 km. Figure 8a shows the volumetric change rates per square kilometre using only the tiles with RTSs present. The volumetric change densities over the total study ~~region~~site strongly depends on the exact outline of study ~~regions~~sites and removing tiles without RTSs present gives a more consistent and comparable volumetric change
285 rate density. To make this more visible the amount of tiles with RTSs present and without can be seen in Figure 8b. Here for example, the Chukotka Peninsula has only a small number of tiles with RTSs present.

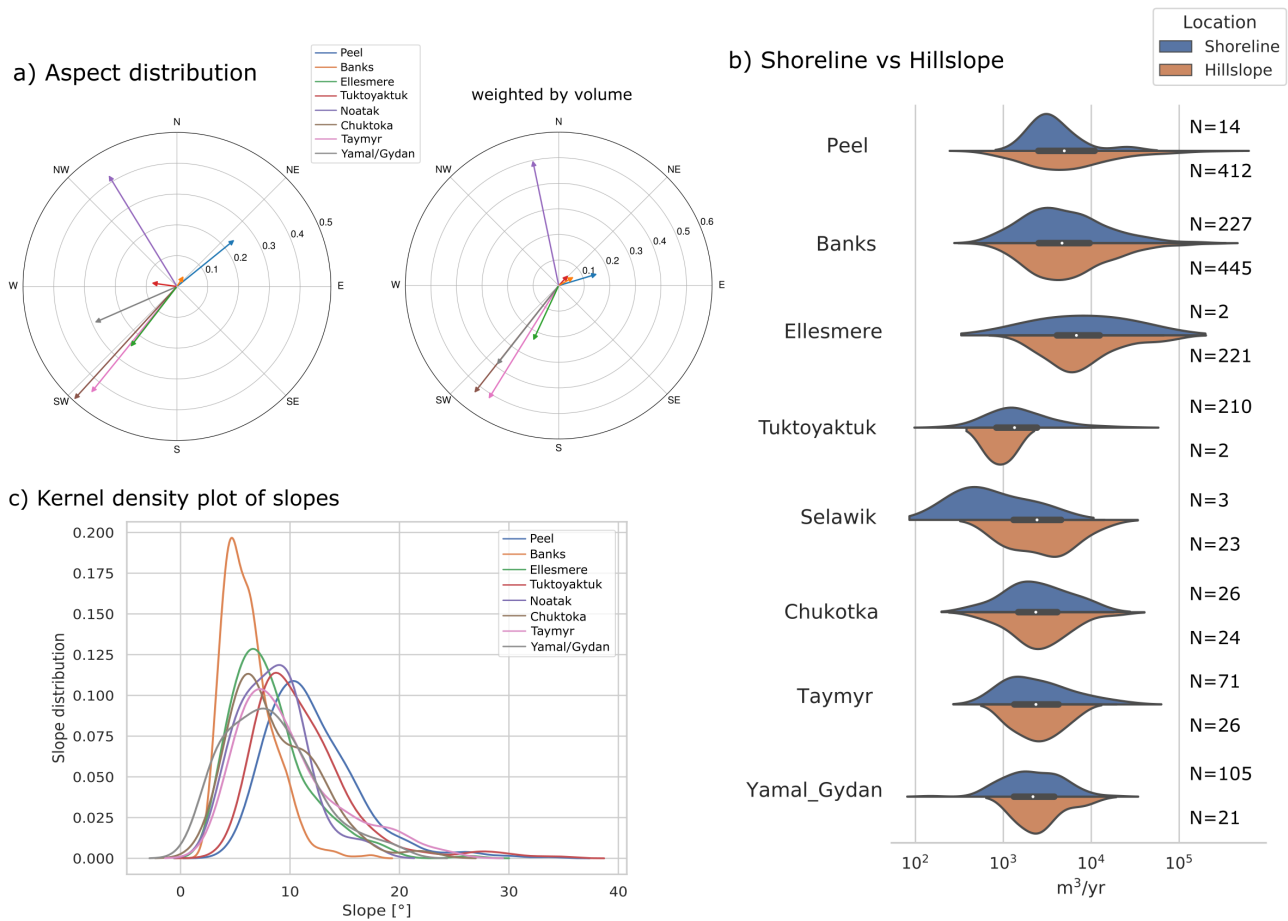


Figure 7. Terrain controls of mapped RTSs for each [regionstudy site](#). (a) shows the aspect main orientation of RTSs in each [region study site](#) (left) and additionally weighted by the volumetric change rates (right). (b) shows the probability density distributions of volumetric changes rates [separated by RTS location in form of a violin plot](#). On [The top part of each violin indicates the rightside subset of shoreline RTSs](#) and the [Number bottom part the subset of hillslope RTS](#) as [probability density of the data across the distribution of values smoothed by a kernel density estimator](#). For each violin plot the white dot on the center line indicates the mean value of the entire study site dataset with the thick center line showing the interquartile range. The number of RTSs in each [subsample subset](#) is listed [on the right](#). Some [areas sites](#) are dominated by one location type. (c) shows the distribution of the pre-disturbed DEM slopes at the RTS locations.

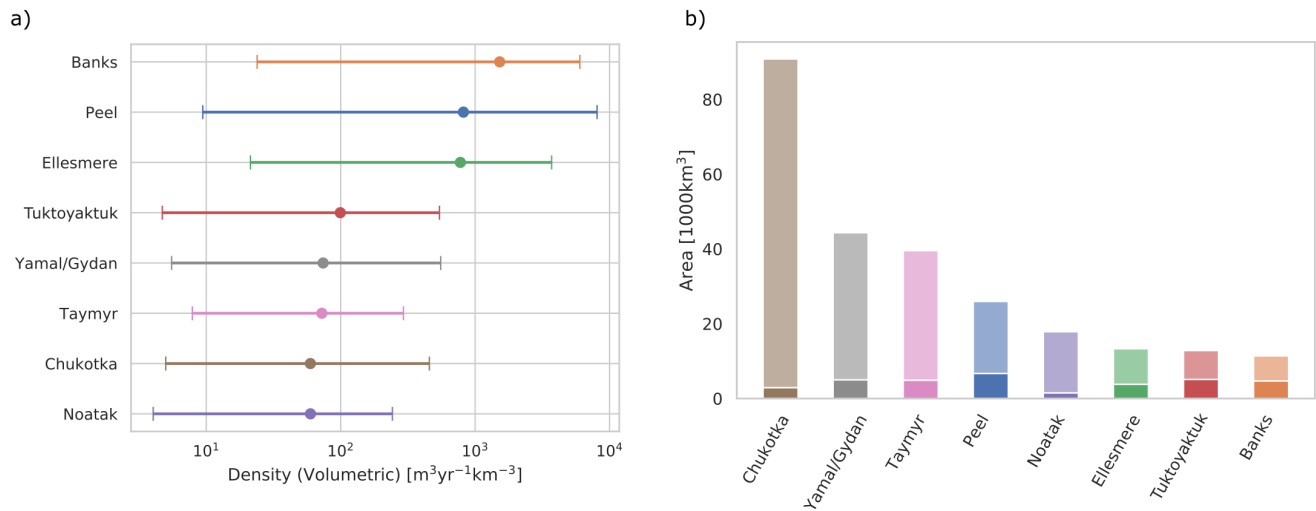


Figure 8. Volumetric change rate densities and density related to study site size for each study site. a) shows the computed RTS volumetric change rate densities using a 10 km 10 km by 10 km 10 km grid with the empty grid cells removed. The vertical bars indicate the range in the computed densities. (b) shows the study region-site size in transparent with the fraction of tiles with RTS present in solid (b).

5 Discussion

5.1 Probability density functions to characterize thaw slump activity

The computed probability density functions of the yearly area and volumetric change rates follow a characteristic inverse gamma law with first an increase in frequency up to a maximum value with the most abundant thaw slump sizes (rollover) and then a decrease with an exponential decay tail above a certain cutoff value. Our findings show that the applicability of this universal scaling also applies to permafrost landscapes, despite differences in the governing geomorphic processes with respect to lower latitude environments. ~~It should be emphasized here~~ Here we emphasize again that ~~of our analyses to common landslides~~ between our analyses and that of common landslide studies is that RTSs are a multi-year phenomena with variable yearly erosion rates. Some variability in the exact form of the distributions should therefore be expected if different time periods are chosen.

To further investigate the distributions we distinguish between two parts: (1) the exponential decay part for large RTSs and (2) the part that deviate from this exponential decay below the cutoff point. For landslides the exponential decay part is typically explained in a statistical way by the concept of self-organized criticality, where a constant "input" of a specific landslide size at random location, together with a merger of landslides that are close to each other, reproduces this distribution (Bak and Tang, 1989; Turcotte, 1999). For RTSs this explanation seems plausible since initiation and evolution are strongly linked to soil properties that can promote RTS development in close proximity and also RTS coalescence is common (Lantz and Kokelj, 2008; Lantuit et al., 2012; Wang et al., 2016). In addition to the universal exponential decay behaviour in all study ~~regions-sites~~ regions-sites we found that the largest RTSs in the Peel, Banks and Ellesmere study ~~regions-sites~~ regions-sites have order of magnitudes larger growth rates (Figure 5 a,b). A possible explanation is that topographic and geomorphological properties, like the amount of massive ice, overburden thickness or the steepness of terrain only allow RTSs to grow to a certain size (Kokelj et al., 2017; Rudy et al., 2017; Jones et al., 2019). For example in the Tuktoyaktuk study ~~region-site~~ region-site ($N_{RTS} = 212$) ~~were where~~ were where RTSs occur at lakeshores in mainly flat regions, the largest RTSs show growth rates ~~of $5200\text{ m}^2\text{ yr}^{-1}$ and $31800\text{ m}^3\text{ yr}^{-1}$ compared to for example the Ellesmere region~~ between $5200\text{ m}^2\text{ yr}^{-1}$ and $31800\text{ m}^3\text{ yr}^{-1}$ compared to, for example, the Ellesmere site ($N_{RTS} = 223$) with more topographic features and mainly hillslope RTSs which shows 3 ~~to~~ to 4 times higher maximum growth rates (~~$23000\text{ m}^2\text{ yr}^{-1}$ and $106400\text{ m}^3\text{ yr}^{-1}$~~ range is between $23000\text{ m}^2\text{ yr}^{-1}$ and $106400\text{ m}^3\text{ yr}^{-1}$). This suggests that additional to the exponential decay factor also a maximum RTS growth rate is important to characterize the high end tail of the probability density function. For the deviation from the exponential decay, two types of explanation have been proposed for landslides in temperate climate (Tebbens, 2020). First an under-sampling of small landslides due to limitations in resolution and secondly an explanation that attributes this divergence on physical processes. By investigating our dataset a divergence due to under-sampling seems unlikely since the PDFs in Peel, Banks and, Ellesmere show this divergence (cutoff-point) at high yearly change rates of ~~$>10^4\text{ m}^2\text{ yr}^{-1}$ and $>3 \cdot 10^4\text{ m}^3\text{ yr}^{-1}$~~ $>10^4\text{ m}^2\text{ yr}^{-1}$ and $>3 \cdot 10^4\text{ m}^3\text{ yr}^{-1}$ which corresponds to area and volumetric changes high above the resolution limit (TanDEM-X ~~resolution: Spatial~~ DEM resolution: Horizontal $\approx 10\text{ m}$, vertical ~~$2-5\text{ m}$~~ 2 to 5 m). The physical origins are likely related to environmental conditions and ~~soil-properties~~ physical characteristics of ground materials like

320 ground ice-content but are outside the scope of this work. Future models for thaw slump initiation and evolution should be able to investigate the drivers and reproduce such distributions.

5.2 Similarities and differences in Area-Volume scaling

We found a power law relationship ($V \approx A^\alpha$) between the area and the volumetric change rates with a scaling coefficients α of 1.15 for the total dataset and ranging between 1.05 and 1.37 for the individual regions-study sites. Such relationship are
325 known from landslides in temperate climates with typically values of 1 to 1.5 (Larsen et al., 2010; Klar et al., 2011). For RTSs only one study by Kokelj et al. (2021), investigating thaw-slumps-RTSs on the Peel Plateau and Richardson Mountains, has estimated this relationship and found a scaling coefficient of 1.42 which is relatively high compared to our values (Peel: 1.27, Tuktoyaktuk: 1.17) but inside the estimated error.

Comparing the coefficients between regions-study sites we found that lower scaling coefficients are not correlated with smaller
330 slumps-RTSs. For example the scaling law coefficient in the Tuktoyaktuk region-site with relatively small slumps-RTSs is the same as for the RTSs in the Ellesmere region-site with the largest slumps-RTSs in our dataset. On the other hand, for RTSs in the Peel Plateau-there is only study site there is little confining topography and deep layers of ice-rich tills which allows the headwall that allow the headwalls to grow to large sizes and consequently yield a steeper regression curve (Lacelle et al., 2015). The diversity in landform characteristics also contributes to the scaling-relationship-variation of the area to volume
335 scaling coefficient. In the study regions-Banks-Island-sites Banks or Noatak, shallow detachments are dominant in the small-area range. They-These may promote larger scaling coefficients when combined with older, deeper thaw-slumps-RTSs (Lewkowicz, 1987b). Furthermore, most RTSs initiate as shallow active layer detachments. The gradual transition-following-an-extreme increase in headwall heights following the initiation event could lead to a temporal change in the scaling coefficient. Further investigations relating the scaling coefficients to additional RTS and area characteristics (e.g. soil properties, climatic history,
340 age of the RTSs) are needed.

5.3 Terrain controls and their relation to RTS size

With the available data we could determine several terrain controls, namely the orientation of thaw-slump-RTS growth, the slope of the predisturbed area the slumps-RTS grew into as well as the location in terms of hillslope and shoreline RTSs. Our findings in terms of the preferred orientation of RTSs are mostly consistent with past regional studies: A preferred South-
345 West orientation for RTSs in the Siberian study regions-sites (Nesterova et al., 2019) and Ellesmere Island (Jones et al., 2019), towards the North-East for the Peel Plateau-study-region-study site (Lacelle et al., 2015) and North facing RTSs in the-Noatak-Valley-Noatak (Swanson and Nolan, 2018). For RTSs in the Tuktoyaktuk region-study site we found no preferred orientation consistent with Wang et al. (2009), but in contradiction to other studies that found RTSs orientations that favour North facing slopes (Kokelj et al., 2009; Zwieback et al., 2018, 2020). The association with aspect hints at inter-regional
350 differences in the governing geomorphic drivers and controls. A South-West facing orientation is considered to be related to higher initiation- and growth-rates of RTSs due to the higher energy available from solar radiation (Lewkowicz, 1987a). This would suggest that solar radiation is an important factor in RTS growth and initiation for the study regions-sites in Ellesmere

and Siberia. Past studies have shown that a high ground ice content is a necessary condition for RTS development (Kokelj and Jorgenson, 2013; Ramage et al., 2017). During the Holocene Thermal Maximum the regions in North-West Canada experienced warmer summer temperatures than other Arctic regions and could have removed ground ice on South-facing slopes (Burn et al., 1986; Kaufman et al., 2004; Lacelle et al., 2010; Zwieback et al., 2018). Thus the differences in RTS aspect distributions could be related to the climatic history. For example the dominant North-facing exposure on the Peel Plateau could reflect such anisotropic abundance of ground ice.

We did not find a significant relation between thaw-slump-RTS size (area and volumetric change rates) to aspect as well as slope or location (hillslope, shoreline). This finding affirms previous studies that highlighted the complexity of the processes and controls governing thaw-slump-RTS expansion.

5.4 Implications

The scaling relations we quantified are critical for modelling and predicting thaw-slumping-and-its-impact-RTS activity and the impacts on biogeochemical cycling. The regional variability in scaling behaviour needs to be considered when upscaling field observations to estimate large-scale nutrient, sediment, and carbon budgets. Because Earth system models strive to capture the variability of these processes from regional to global scales, our results can be used to calibrate and validate global models. Possible changes in the scaling relations could be important indicators to predict future thaw-slump-RTS evolution and impacts. Our observations of variable thaw-slump-RTS development rates and regimes highlight the need for continual pan-Arctic monitoring and further satellite missions to derive high resolution DEMs. The TanDEM-X data availability only allowed us to compute elevation changes in a 4 to 5 year time window. To investigate changes in thaw-slump-RTS activity related to climate change a higher temporal resolution is needed. Here additional observations from the TanDEM-X satellite as well as data from the ArcticDEM could add additional datapoints (Bachmann et al., 2018; Dai et al., 2020). Furthermore, with the derived area-to-volume scaling laws it is potentially possible to use optical satellite images which are available at a higher temporal resolution to estimate the volumetric change.

6 Conclusions

In this study we quantified the yearly volumetric and area change rates of RTSs over a 4 to 5 year time-frame in 10 study regions sites across the Arctic with a total study size of 220 000 km² and a total number of 1868 RTSs. We found that the frequency distributions of the volumetric and area change rates are well described by an Inverse Gamma distribution ($R^2 > 0.5$) with the distinct features of a rollover, cutoff and an exponential decay for large RTSs. This kind of behaviour is well known for landslides in temperate climate regions with very different trigger mechanisms and soil properties and could provide valuable insights in modelling future RTS evolution on a pan-Arctic scale.

The comparison between regions-study sites showed that the distribution of RTSs in three study regions-sites in northern Canada (Peel Plateau and Richardson Mountains, Banks Island, Ellesmere Island) are shifted towards higher change rates in volume and area. Nevertheless, the exponential decay rates for large RTSs in all regions-study sites were similar.

385 Our analyses revealed consistent but regionally variable area-to-volume scaling behaviour. For the total dataset we found a scaling coefficient of $\gamma = 1.15 \pm 0.01$ $\alpha = 1.15 \pm 0.01$ with some variance between the study ~~regions~~ ($\gamma = 1.05 - 1.37$) ~~sites~~ (α between 1.05 to 1.37).

For the aspect we found diverse preferred orientations of RTSs between the study ~~regions~~ ~~sites~~ from no dominant orientation for Tuktoyaktuk and Banks ~~Island~~, a North-East orientation for ~~Peel~~ the Peel Plateau and Richardson Mountains, East-facing
390 ~~RTS in the Notak valley~~ RTSs in the Noatak Valley and a strong South-West orientation of all study ~~regions~~ ~~sites~~ in Siberia and the study ~~region in Ellesmere~~ site on Ellesmere Island.

Our regionally variable ~~thaw slump~~ RTS scaling relations may be used to constrain large-scale estimates of carbon, sediment and nutrient budgets. By capturing the variability of ~~thaw slump~~ RTS change rates across scales, remote sensing is a vital tool for predicting hazards and attendant ecosystem changes in a rapidly changing Arctic.

395 *Data availability.* Locations and extracted properties of RTSs are available at: <https://www.doi.org/10.3929/ethz-b-000482449>. The polygons outlining the area of elevation change are available upon request. Sentinel-2 are available from the Copernicus Open Access Hub (<https://scihub.copernicus.eu>). TanDEM-X CoSSC data are not freely available but can be requested from the German Aerospace Center (DLR) and accessed through the EOWEB (<https://eoweb.dlr.de>)

Author contributions. PB conducted the DEM processing, analysed the data and drafted the initial manuscript, SZ provided critical guidance
400 and contributed to the writing of the manuscript, NB and PB conducted the manual RTS mapping, IH provided guidance and corrections to the final manuscript.

Competing interests. The authors declare no conflict of interest

References

- Bachmann, M., Borla Tridon, D., Martone, M., Sica, F., Buckreuss, S., and Zink, M.: How to update a global DEM - acquisition concepts
405 for TanDEM-X and tandem-L, in: Proceedings of the European Conference on Synthetic Aperture Radar, EUSAR 2018, 2018.
- Bak, P. and Tang, C.: Earthquakes as a self-organized critical phenomenon, *Journal of Geophysical Research: Solid Earth*, 94, 15 635–15 637, 1989.
- Balser, A. W., Jones, J. B., and Gens, R.: Timing of retrogressive thaw slump initiation in the Noatak Basin, northwest Alaska, USA, *Journal of Geophysical Research: Earth Surface*, 119, 1106–1120, <https://doi.org/10.1002/2013JF002889>, 2014.
- 410 Bennett, G., Molnar, P., Eisenbeiss, H., and McArdell, B.: Erosional power in the Swiss Alps: characterization of slope failure in the Illgraben, *Earth Surface Processes and Landforms*, 37, 1627–1640, <https://doi.org/10.1002/esp.3263>, 2012.
- Bernhard, P., Zwieback, S., Leinss, S., and Hajnsek, I.: Mapping Retrogressive Thaw Slumps Using Single-Pass TanDEM-X Observations, *IEEE Journal of Selected Topics in Applied Earth Observations and Remote Sensing*, 13, 3263–3280, <https://doi.org/10.1109/JSTARS.2020.3000648>, 2020.
- 415 Boggs, P. T. and Rogers, J. E.: Orthogonal Distance Regression, *Statistical analysis of measurement error models and applications: proceedings of the AMS-IMS-SIAM joint summer research conference held June 10-16, 1989*, 112, 186, 1990.
- Brown, J., Ferrians, O., Heginbottom, J. A., and Melnikov, E.: Circum-Arctic Map of Permafrost and Ground-Ice Conditions, Version 2, Boulder, Colorado USA. NSIDC: National Snow and Ice Data Center, <https://doi.org/10.7265/skbg-kf16>, 2002.
- Burn, C. R. and Lewkowicz, A.: Canadian landform examples-17 retrogressive thaw slumps, *Canadian Geographer/Le Géographe canadien*,
420 34, 273–276, 1990.
- Burn, C. R., Michel, F. A., and Smith, M. W.: Stratigraphic, isotopic, and mineralogical evidence for an early Holocene thaw unconformity at Mayo, Yukon Territory, *Canadian Journal of Earth Sciences*, 23, 794–803, <https://doi.org/10.1139/e86-081>, 1986.
- Clauset, A., Shalizi, C. R., and Newman, M. E.: Power-law distributions in empirical data, *SIAM review*, 51, 661–703, 2009.
- Dai, C., Jones, M., Howat, I., Liljedahl, A., Lewkowicz, A., and Freymueller, J.: Using ArcticDEM to identify and quan-
425 tify pan-Arctic retrogressive thaw slump activity, in: EGU General Assembly 2020 Online, 4–8 May 2020 EGU2020-12142, <https://doi.org/10.5194/egusphere-egu2020-12142>, 2020.
- Fritz, T., Rossi, C., Yague-Martinez, N., Rodriguez-Gonzalez, F., Lachaise, M., and Breit, H.: Interferometric processing of TanDEM-X data, in: 2011 IEEE International Geoscience and Remote Sensing Symposium, pp. 2428–2431, <https://doi.org/10.1109/IGARSS.2011.6049701>, 2011.
- 430 Gooseff, M. N., Balser, A., Bowden, W. B., and Jones, J. B.: Effects of hillslope thermokarst in northern Alaska, *Eos, Transactions American Geophysical Union*, 90, 29–30, 2009.
- Grosse, G., Harden, J., Turetsky, M., McGuire, A. D., Camill, P., Tarnocai, C., Frohling, S., Schuur, E. A., Jorgenson, T., Marchenko, S., Romanovsky, V., Wickland, K. P., French, N., Waldrop, M., Bourgeau-Chavez, L., and Striegl, R. G.: Vulnerability of high-latitude soil organic carbon in North America to disturbance, *Journal of Geophysical Research: Biogeosciences*, <https://doi.org/10.1029/2010JG001507>,
435 2011.
- Jones, M. K. W., Pollard, W. H., and Jones, B. M.: Rapid initialization of retrogressive thaw slumps in the Canadian high Arctic and their response to climate and terrain factors, *Environmental Research Letters*, 14, 055 006, 2019.
- Kang-tsung, C. and Bor-wen, T.: The Effect of DEM Resolution on Slope and Aspect Mapping, *Cartography and Geographic Information Systems*, 18, 69–77, <https://doi.org/10.1559/152304091783805626>, 1991.

- 440 Kaplan, G. and Avdan, U.: Object-based water body extraction model using Sentinel-2 satellite imagery, *European Journal of Remote Sensing*, <https://doi.org/10.1080/22797254.2017.1297540>, 2017.
- Kaufman, D., Ager, T., Anderson, N., Anderson, P., Andrews, J., Bartlein, P., Brubaker, L., Coats, L., Cwynar, L., Duvall, M., Dyke, A., Edwards, M., Eisner, W., Gajewski, K., Geirsdóttir, A., Hu, F., Jennings, A., Kaplan, M., Kerwin, M., Lozhkin, A., MacDonald, G., Miller, G., Mock, C., Oswald, W., Otto-Bliesner, B., Porinchu, D., Rühland, K., Smol, J., Steig, E., and Wolfe, B.: Holocene thermal maximum
445 in the western Arctic (0–180W), *Quaternary Science Reviews*, 23, 529 – 560, <https://doi.org/10.1016/j.quascirev.2003.09.007>, 2004.
- Klar, A., Aharonov, E., Kalderon-Asael, B., and Katz, O.: Analytical and observational relations between landslide volume and surface area, *Journal of Geophysical Research: Earth Surface*, 116, 2011.
- Kokelj, S. V. and Jorgenson, M. T.: Advances in thermokarst research, *Permafrost and Periglacial Processes*, 24, 108–119, <https://doi.org/10.1002/ppp.1779>, 2013.
- 450 Kokelj, S. V., Lantz, T. C., Kanigan, J., Smith, S. L., and Coutts, R.: Origin and polycyclic behaviour of tundra thaw slumps, Mackenzie Delta region, Northwest Territories, Canada, *Permafrost and Periglacial Processes*, 20, 173–184, <https://doi.org/10.1002/ppp.642>, 2009.
- Kokelj, S. V., Lantz, T. C., Tunnicliffe, J., Segal, R., and Lacelle, D.: Climate-driven thaw of permafrost preserved glacial landscapes, northwestern Canada, *Geology*, 45, 371–374, <https://doi.org/10.1130/G38626.1>, 2017.
- Kokelj, S. V., Kokoszka, J., van der Sluijs, J., Rudy, A. C. A., Tunnicliffe, J., Shakil, S., Tank, S. E., and Zolkos, S.: Thaw-driven mass
455 wasting couples slopes with downstream systems, and effects propagate through Arctic drainage networks, *The Cryosphere*, 15, 3059–3081, <https://doi.org/10.5194/tc-15-3059-2021>, 2021.
- Krieger, G., Moreira, A., Fiedler, H., Hajsek, I., Werner, M., Younis, M., and Zink, M.: TanDEM-X: A satellite formation for high-resolution SAR interferometry, in: *IEEE Transactions on Geoscience and Remote Sensing*, vol. 45, pp. 3317–3340, <https://doi.org/10.1109/TGRS.2007.900693>, 2007.
- 460 Lacelle, D., Bjornson, J., Lauriol, B., Clark, I., and Troutet, Y.: Segregated-intrusive ice of subglacial meltwater origin in retrogressive thaw flow headwalls, Richardson Mountains, NWT, Canada, *Quaternary Science Reviews*, 23, 681 – 696, <https://doi.org/10.1016/j.quascirev.2003.09.005>, 2004.
- Lacelle, D., Bjornson, J., and Lauriol, B.: Climatic and geomorphic factors affecting contemporary (1950-2004) activity of retrogressive thaw slumps on the Aklavik plateau, Richardson mountains, NWT, Canada, *Permafrost and Periglacial Processes*, 21, 1–15,
465 <https://doi.org/10.1002/ppp.666>, 2010.
- Lacelle, D., Brooker, A., Fraser, R. H., and Kokelj, S. V.: Distribution and growth of thaw slumps in the Richardson Mountains-Peel Plateau region, northwestern Canada, *Geomorphology*, 235, 40–51, <https://doi.org/10.1016/j.geomorph.2015.01.024>, 2015.
- Lantuit, H. and Pollard, W. H.: Fifty years of coastal erosion and retrogressive thaw slump activity on Herschel Island, southern Beaufort Sea, Yukon Territory, Canada, *Geomorphology*, 95, 84–102, <https://doi.org/10.1016/j.geomorph.2006.07.040>, 2008.
- 470 Lantuit, H., Pollard, W. H., Couture, N., Fritz, M., Schirrmeyer, L., Meyer, H., and Hubberten, H.-W.: Modern and Late Holocene Retrogressive Thaw Slump Activity on the Yukon Coastal Plain and Herschel Island, Yukon Territory, Canada, *Permafrost and Periglacial Processes*, 23, 39–51, <https://doi.org/10.1002/ppp.1731>, 2012.
- Lantz, T. C. and Kokelj, S. V.: Increasing rates of retrogressive thaw slump activity in the Mackenzie Delta region, N.W.T., Canada, *Geophysical Research Letters*, 35, <https://doi.org/10.1029/2007GL032433>, 2008.
- 475 Larsen, Montgomery, and Korup: Landslide erosion controlled by hillslope material, *Nature Geoscience*, 3, 247–251, 2010.
- Leinss, S. and Bernhard, P.: TanDEM-X: Deriving InSAR height changes and velocity dynamics of great aletsch glacier, *IEEE Journal of Selected Topics in Applied Earth Observations and Remote Sensing*, 14, 4798–4815, 2021.

- Lewkowicz, A. G.: Headwall retreat of ground-ice slumps, Banks Island, Northwest Territories, Canadian Journal of Earth Sciences, <https://doi.org/10.1139/e87-105>, 1987a.
- 480 Lewkowicz, A. G.: Nature and Importance of Thermokarst Processes, Sand Hills Moraine, Banks Island, Canada, Geografiska Annaler: Series A, Physical Geography, 69, 321–327, <https://doi.org/10.1080/04353676.1987.11880218>, 1987b.
- Lewkowicz, A. G. and Way, R. G.: Extremes of summer climate trigger thousands of thermokarst landslides in a High Arctic environment, Nature Communications, <https://doi.org/10.1038/s41467-019-09314-7>, 2019.
- Malamud, B. D., Turcotte, D. L., Guzzetti, F., and Reichenbach, P.: Landslide inventories and their statistical properties, Earth Surface Processes and Landforms, 29, 687–711, <https://doi.org/10.1002/esp.1064>, 2004.
- 485 Markovsky, I. and Van Huffel, S.: Overview of total least-squares methods, Signal Processing, 87, 2283 – 2302, <https://doi.org/10.1016/j.sigpro.2007.04.004>, special Section: Total Least Squares and Errors-in-Variables Modeling, 2007.
- Martone, M., Bräutigam, B., Rizzoli, P., Gonzalez, C., Bachmann, M., and Krieger, G.: Coherence evaluation of TanDEM-X interferometric data, ISPRS Journal of Photogrammetry and Remote Sensing, 73, 21–29, <https://doi.org/https://doi.org/10.1016/j.isprsjprs.2012.06.006>,
- 490 innovative Applications of SAR Interferometry from modern Satellite Sensors, 2012.
- McFeeters, S. K.: The use of the Normalized Difference Water Index (NDWI) in the delineation of open water features, International Journal of Remote Sensing, <https://doi.org/10.1080/01431169608948714>, 1996.
- Millan, R., Dehecq, A., Trouvé, E., Gourmelen, N., and Berthier, E.: Elevation changes and X-band ice and snow penetration inferred from TanDEM-X data of the Mont-Blanc area, in: 2015 8th International Workshop on the Analysis of Multitemporal Remote Sensing Images (Multi-Temp), pp. 1–4, <https://doi.org/10.1109/Multi-Temp.2015.7245753>, 2015.
- 495 Nesterova, N., Khomutov, A., Kalyukina, A., and Leibman, M.: The specificity of thermal denudation feature distribution on Yamal and Gydan peninsulas Russia, in: EGU General Assembly 2020 Online, 4–8 May 2020, EGU2020-746, <https://doi.org/10.5194/egusphere-egu2020-746>, 2019.
- Nicu, I. C., Lombardo, L., and Rubensdotter, L.: Preliminary assessment of thaw slump hazard to Arctic cultural heritage in Nordenskiöld Land, Svalbard, Landslides, pp. 1–13, 2021.
- 500 Nitze, I., Grosse, G., Jones, B. M., Arp, C. D., Ulrich, M., Fedorov, A., and Veremeeva, A.: Landsat-based trend analysis of lake dynamics across Northern Permafrost Regions, Remote Sensing, 9, <https://doi.org/10.3390/rs9070640>, 2017.
- Nitze, I., Grosse, G., Jones, B., Romanovsky, V., and Boike, J.: Remote sensing quantifies widespread abundance of permafrost region disturbances across the Arctic and Subarctic, Nature communications, 9, 1–11, 2018.
- 505 Obu, J.: How Much of the Earth's Surface is Underlain by Permafrost?, Journal of Geophysical Research: Earth Surface, 126, e2021JF006123, <https://doi.org/https://doi.org/10.1029/2021JF006123>, e2021JF006123 2021JF006123, 2021.
- Ohtani, K.: Bootstrapping R2 and adjusted R2 in regression analysis, Economic Modelling, 17, 473–483, [https://doi.org/10.1016/S0264-9993\(99\)00034-6](https://doi.org/10.1016/S0264-9993(99)00034-6), 2000.
- Parker, R., Hancox, G., Petley, D., Massey, C., Densmore, A., and Rosser, N.: Spatial distributions of earthquake-induced landslides and hillslope preconditioning in northwest South Island, New Zealand., Earth surface dynamics., 3, 501–525, 2015.
- 510 Planet-Team: Planet Application Program Interface: In Space for Life on Earth, <https://api.planet.com>, 2018.
- Ramage, J. L., Irrgang, A. M., Herzsuh, U., Morgenstern, A., Couture, N., and Lantuit, H.: Terrain Controls on the Occurrence of Coastal Retrogressive Thaw Slumps along the Yukon Coast, Canada, Journal of Geophysical Research: Earth Surface, <https://doi.org/10.1002/2017JF004231>, 2017.

- 515 Rudy, A. C., Lamoureux, S. F., Kokelj, S. V., Smith, I. R., and England, J. H.: Accelerating Thermokarst Transforms Ice-Cored Terrain Triggering a Downstream Cascade to the Ocean, *Geophysical Research Letters*, <https://doi.org/10.1002/2017GL074912>, 2017.
- Schuur, E. A. G., McGuire, A. D., Schädel, C., Grosse, G., Harden, J. W., Hayes, D. J., Hugelius, G., Koven, C. D., Kuhry, P., Lawrence, D. M., Natali, S. M., Olefeldt, D., Romanovsky, V. E., Schaefer, K., Turetsky, M. R., Treat, C. C., and Vonk, J. E.: Climate change and the permafrost carbon feedback, *Nature*, 520, <https://doi.org/10.1038/nature14338>, 2015.
- 520 Segal, R. A., Lantz, T. C., and Kokelj, S. V.: Acceleration of thaw slump activity in glaciated landscapes of the Western Canadian Arctic, *Environmental Research Letters*, 11, 034 025, <https://doi.org/10.1088/1748-9326/11/3/034025>, 2016.
- Swanson, D. K. and Nolan, M.: Growth of retrogressive thaw slumps in the Noatak Valley, Alaska, 2010-2016, measured by airborne photogrammetry, *Remote Sensing*, <https://doi.org/10.3390/rs10070983>, 2018.
- Tanyaş, H., Allstadt, K. E., and van Westen, C. J.: An updated method for estimating landslide-event magnitude, *Earth Surface Processes and Landforms*, 43, 1836–1847, <https://doi.org/10.1002/esp.4359>, 2018.
- 525 Tebbens, S. F.: Landslide Scaling: A Review, *Earth and Space Science*, 7, e2019EA000 662, <https://doi.org/10.1029/2019EA000662>, e2019EA000662 2019EA000662, 2020.
- Turcotte, D. L.: Self-organized criticality, *Reports on progress in physics*, 62, 1377, 1999.
- Turetsky, M. R., Abbott, B. W., Jones, M. C., Anthony, K. W., Olefeldt, D., Schuur, E. A., Grosse, G., Kuhry, P., Hugelius, G., Koven, C.,
530 et al.: Carbon release through abrupt permafrost thaw, *Nature Geoscience*, 13, 138–143, 2020.
- Van der Sluijs, J., Kokelj, S. V., Fraser, R. H., Tunnicliffe, J., and Lacelle, D.: Permafrost terrain dynamics and infrastructure impacts revealed by UAV photogrammetry and thermal imaging, *Remote Sensing*, 10, 1734, 2018.
- Wang, B., Paudel, B., and Li, H.: Retrogression characteristics of landslides in fine-grained permafrost soils, Mackenzie Valley, Canada, *Landslides*, 6, 121–127, 2009.
- 535 Wang, B., Paudel, B., and Li, H.: Behaviour of retrogressive thaw slumps in northern Canada—three-year monitoring results from 18 sites, *Landslides*, 13, 1–8, 2016.
- Werner, C., Wegmueller, U., Strozzi, T., and Wiesmann, A.: GAMMA SAR and interferometric processing software, in: European Space Agency, (Special Publication) ESA SP, 461, pp. 211–219, 2000.
- Zwieback, S., Kokelj, S., Günther, F., Boike, J., Grosse, G., and Hajnsek, I.: Sub-seasonal thaw slump mass wasting is not consistently energy
540 limited at the landscape scale, *Cryosphere*, <https://doi.org/10.5194/tc-12-549-2018>, 2018.
- Zwieback, S., Boike, J., Marsh, P., and Berg, A.: Debris cover on thaw slumps and its insulative role in a warming climate, *Earth Surface Processes and Landforms*, 45, 2631–2646, <https://doi.org/10.1002/esp.4919>, 2020.